



Novel analytical heat source model for cold rolling based on an energy method and unified yield criterion

Yufeng Zhang^{1,2} · Xu Li^{1,2} · Meiyong Zhao² · Fuquan Qu^{1,2} · Yuhe Zhang³ · Wen Peng^{1,2} · Dewen Zhao^{1,2} · Hongshuang Di^{1,2} · Dianhua Zhang^{1,2}

Received: 11 May 2022 / Accepted: 21 August 2022 / Published online: 16 September 2022
© The Author(s), under exclusive licence to Springer-Verlag London Ltd., part of Springer Nature 2022

Abstract

Accurate calculation of the heat source in the roll gap during the cold rolling process is the basis for a well-designed coolant system, which is particularly important for reducing roll wear and improving the flatness quality of strip steel. Although many established numerical models have high precision when calculating the work roll temperature, complex modeling processes and large calculation times result in the inability to predict the work roll temperature quickly for the application of automatic control systems. Therefore, the authors developed a new analytical heat source model to calculate the axial temperature distribution of the work roll in the cold rolling process. First, according to the deformation characteristics of strip cold rolling, the deformation zone is divided into a plastic zone and two elastic zones, and the length of each deformation zone is calculated considering the effect of tension. Then, the friction heat generated in the elastic zone is calculated. Second, new exponential velocity and corresponding strain-rate fields satisfying kinematically admissible conditions are proposed to calculate the deformation heat and friction heat generated in the plastic zone. Finally, the work roll temperature prediction model is established by contemplating the heat source of the roll gap, emulsion heat transfer, air cooling, and contact heat transfer with the intermediate roll. By repeatedly optimizing the weighted coefficient d of intermediate principal shear stress on the yield criterion, the maximum error between the calculated results and the actual measured cold roll temperature data was reduced to 3.1%. The effects of the reduction ratio, rolling speed, and resistance to deformation on the deformation heat and friction heat are discussed, and the variation of temperature field of the work roll with time is analyzed quantitatively.

Keywords Cold rolling · Energy method · Friction heat · Deformation heat · UY criterion, Temperature field

Abbreviations

h_{in}, h_{out} Half of the initial and final strip thickness at entry and exit respectively
 h_0, h_1 Half of the initial and final strip thickness at entry and exit in plastic zone
 h_{mb}, h_{mf} Half of the average strip thickness in backward and forward slip zone

$\Delta h_{in}, \Delta h_{out}$ Half of the reduction in elastic deformation and recovery zones respectively
 h_x, h_α Half of the strip thickness during plastic deformation process
 E_s, E_w Young's modulus of strip and roll
 ν_s, ν_w Poisson ratio of strip and roll
 $\sigma_{s\,in}, \sigma_{s\,out}$ Resistance of strip deformation at entry and exit sides
 σ_b, σ_f Backward and forward tension stresses
 Δh Half of the reduction in plastic zone
 R Original radius of the work roll
 R_0 Flattened roll radius of work roll
 l Projected length of roll-strip contact arc in plastic deformation zone
 w Strip width
 θ Bite angle
 α Contact angle
 α_n Neutral angle

✉ Hongshuang Di
dhshuang@mail.neu.edu.cn

¹ The State Key Laboratory of Rolling and Automation, Northeastern University, 110819 Shenyang, Liaoning, People's Republic of China

² School of Materials Science and Engineering, Northeastern University, 110819 Shenyang, Liaoning, People's Republic of China

³ Baogang Group, 014000 Baotou, Inner Mongolia, People's Republic of China

F_{in}^e	Roll separating force of elastic deformation zone
F_{out}^e	Roll separating force of elastic recovery zone
U	Flow volume per second
μ	Friction coefficient
$D(\dot{\epsilon}_{ij})$	The power per unit volume
v_0	Entrance velocity
v_R	Roll speed
d	Yield criterion parameter
σ_s	Material yield stress
τ_f	Friction stress
k	Yield shear stress, $k = \sigma_s / \sqrt{3}$
\dot{W}_i	Internal plastic deformation power
\dot{W}_f^e, \dot{W}_f^p	Friction power
Q_f^e, Q_f^p	Friction heat generated in the elastic zone and plastic zone
Q_i	Deformation heat
Q_e, Q_a, Q_{inter}	Heat exchange between the work roll with emulsion, air, and intermediate roll
t_r^e, t_r^p	Contact time between roll with strip in the elastic zone and plastic zone
t_{we}, t_{wa}, t_{wi}	Contact time between the roll with emulsion, air and intermediate roll

1 Introduction

The strip flatness control problem in the continuous cold rolling process is one of the most complex control processes in the industrial control field due to its multivariable, multi-control-loop, nonlinear, and strongly coupled characteristics [1]. An accurate flatness prediction model is important for improving the level of flatness control. The calculation accuracy of the strip flatness of cold rolling depends on the calculation accuracy of the roll system's elastic deformation, but the thermal deformation of the rolls and other time-varying factors during the rolling process also have a significant impact on the control of the strip flatness control. In the cold rolling process, the surfaces of the work rolls are subjected repeatedly to heat transfer from the strip from the roll gap and the cooling caused by the emulsion; so, the surface temperature changes periodically, which causes thermal expansion of the rolls and affects the strip flatness. Therefore, an accurate heat source model of the roll gap is a prerequisite for calculating the thermal deformation of the rolls. It would be of enormous significance for the design of a fine coolant system and the improvement of the strip shape quality if the temperature of the cold roll could be predicted accurately under different process conditions.

Research on roll thermal behavior began in the early 1960s, and previous research mainly focused on the prediction of the thermal stress and roller life [2]. Until the

early 1980s, most investigators preferred to use numerical and experimental solutions to study the roll thermal behavior, and many research results and test cases were obtained [3]. Wilmotte and Mignon [4] established an axisymmetric finite difference model to study the axial mean value of the roll thermal expansion in 1973. The results showed that the roll axial thermal expansion was a flat bell curve in the corresponding strip width range. In 1978, Lahoti et al. [5] performed a preliminary analysis of the transverse temperature distribution of the strip in the bite zone during the strip rolling process. Nakagawa [6] used a three-dimensional Lagrangian finite difference model to study the transient establishment process of the roll thermal crown, and determined that the reduction, strip temperature, and cooling condition are three major influential factors. In 1984, Tseng [7] used the finite difference method (FDM) to calculate the temperature distributions of the roll and strip, and obtained a combined numerical-analytical model. Then, Tseng et al. [8] tried to use the separation variables method to calculate the transient temperature distribution of the roll and strip. The compatibility conditions of two heat conduction models on the contact interface between the roll and the strip were determined by this model, which could be used to conveniently study influences of changes in the geometry and the process conditions on the thermal behavior. However, this method assumed that the friction model and the thermal model were isolated from each other and had no direct relationship; so, the model was only applicable to specific situations and was not generalizable. In 1998, Chang [9] developed a simple model for the correlation between the plastic deformation and the thermal effects by combining the FDM and an analytical solution. Zhang et al. [10] proposed a two-dimensional axisymmetric model using the FDM to predict the transient temperature and thermal crown of the work rolls in the hot rolling process. The accuracy of the model was verified by comparing the production data of a 1700 mm hot strip rolling mill. Recently, Yang et al. [11] developed a transient heat source model of the roll gap in the cold rolling process by considering the emulsion heat transfer coefficient and air cooling, and they studied the influence of the heat source on the transient temperature of the cold rolling strip. This was a significant work, but the model did not account for the friction heat in the elastic deformation zone of the roll gap, and thus, it could be further optimized. Generally, using the FDM to calculate the roll temperature is accurate and convenient. However, FDM for the calculation of the roll temperature will produce a high-order model, which needs to be simplified before being applied online.

With the rapid development of computer technology, the finite element method (FEM) has been widely used in the study of roll thermal behavior because of its high solution accuracy and arbitrary mesh partition. Guo et al. [12] used the ANSYS FEM software to simulate the transient

temperature field and thermal crown of rolls by considering the transient thermal contact and complex boundary conditions. The temperature and thermal crown variations of the surface nodes of the rolls were obtained, and the thermal crown results were in good agreement with the measured data. Benasciutti et al. [13] developed a simplified thermal stress prediction method for hot rolling work rolls based on the FEM. The simulation results of the thermal stress were applied to the rolling process FEM model as heat input, and the elastic–plastic evolution characteristics of the elements close to the roll surface in the hot rolling process were analyzed. At present, commercial FEM software can be used to conveniently analyze the temperature field and thermal deformation of the work roll in the rolling process, and the simulation results are very accurate. However, because of the large amounts of modeling and calculation time, the FEM is not suitable for real-time control systems.

At present, the research on temperature field is mainly concentrated in the field of hot rolling. However, the lubrication state of the strip in the deformation zone of hot roughing mill is very poor. Due to the adhesion between the strip and roll, there will be a large relative non-slip area in the rolling process, thus, the friction heat caused by relative sliding between the strip steel and rolls can be ignored. Unlike the hot rolling deformation, in the cold rolling process, the lubrication state of the strip deformation zone is good. Except for a very small range near the neutral point, there will be relative sliding between the strip and the roll, and a large amount of frictional heat will be generated. The coolant medium used in the cold rolling process is also different from that used in hot rolling. Therefore, the established prediction models for the temperature field of a hot rolling work roll are not suitable for cold rolling. For fast online prediction of the work roll temperature in cold rolling process, an analytical model was derived in the present study to accurately calculate the heat source of the roll gap. The strip in the roll gap was divided into a plastic zone and two elastic zones. The energy method was used to establish an exponential velocity field that satisfied kinematically admissible conditions, and the optimized deformation energy model of the roll gap was derived based on the unified yield (UY) criterion. The friction heat models of the elastic and plastic areas in the roll gap were derived by considering the impact of the roll roughness and emulsion lubrication characteristics, respectively. Then, by considering the heat exchange between the work roll and the emulsion, the heat exchange between the work roll and the air, and the heat exchange between the work roll and the intermediate roll, a high-precision prediction model of the work roll temperature in the cold rolling process was established. Based on this model, the calculated values of the work roll temperature were verified by comparison with data measured online, and the variation characteristics of the heat source of the roll gap

under different rolling conditions are discussed. Finally, the variation characteristics of the temperature field of the work roll in different stages of cold rolling were explored, and the temperature variations in the unstable stage of the cold rolling were quantitatively analyzed, providing a basis for designing a reasonable work roll coolant plan.

2 Heat source model of cold rolling process

2.1 Division of deformation zone in the roll gap

In the cold rolling process, the deformation of the strip is mainly compression and extension deformation, and the compression in the thickness direction is almost changed into longitudinal extension. The deformation of the strip will produce a large amount of deformation heat, which together with the frictional heat generated in the roll gap will raise the work roll temperature. The heat source of the roll gap will not only increase the temperature of the work roll and the strip, but will also transfer to the intermediate roll and the supporting roll through heat conduction, and radial and axial heat conduction occur in each roll. In addition, as the roll rotates at a high speed, some heat will be lost through convection with the emulsion and the air; so, the impacts of the above factors on the roll temperature need to be considered. Figure 1 shows the contact between the work roll and different media in the cold rolling process. Based on a reasonable simplification of the actual heat transfer situation on the cold rolling site, we divided the work roll into the roll gap contact zone (zone 1), forced convection zone (zones 3 and 7), free convection zone (zones 2, 4, 6, and 8), and roll contact zone (zone 5) along the circumference. The deformation heat and friction heat generated in zone 1 increase the surface temperature of the work roll, while the other areas are cooling areas of the roll. The heat flow

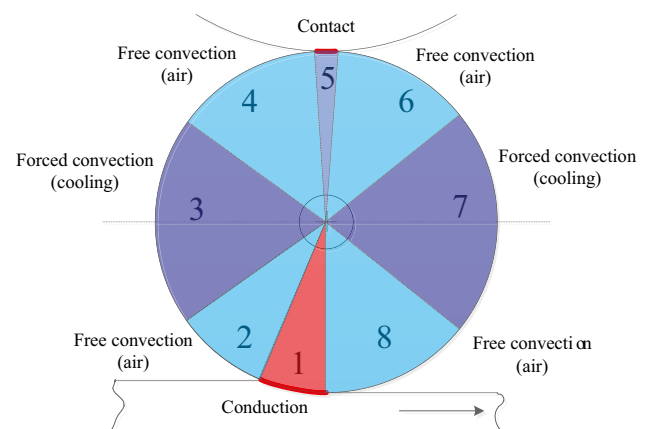


Fig. 1 Zone division along the peripheral direction of the work roll

between each zone and the roll depends on the temperature difference between them.

In addition, because of the large deformation resistance of the material during cold rolling, the roll is significantly flattened, and there is a larger elastic deformation zone compared with that of hot rolling. Thus, zone I in Fig. 1 is divided into entrance elastic deformation zone I, plastic zone II, and elastic recovery zone III, as shown in Fig. 2.

As shown in Fig. 2, the strip is rolled through a pair of cylindrical work rolls with a flattened roll radius R (original radius R_0), and its thickness is reduced from $2h_{in}$ to $2h_{out}$. In plastic zone II, the strip thickness is reduced from $2h_0$ to $2h_1$, the unilateral reduction is $\Delta h = h_0 - h_1$, and l is the projection length of the contact arc in the rolling direction. A coordinate system is set up at the midpoint of the entry cross section of zone II, and the x , y and z axes represent the length, width and thickness directions of the strip, respectively. Owing to the symmetry of the deformation zone, only a quarter of the strip deformation zone is considered. The half thickness and first-order derivative equations of the deformation zone are as follows:

$$\begin{aligned} h_x &= R + h_1 - \sqrt{R^2 - (l-x)^2} \\ h_\alpha &= R + h_1 - R \cos \alpha \end{aligned} \tag{1}$$

$$h'_x = -\frac{l-x}{\sqrt{R^2 - (l-x)^2}} = -\tan \alpha \tag{2}$$

Note that the width-to-thickness ratio is much higher than 10 during cold rolling, and the width spread can be ignored. Then, the cold rolling process can be approximately considered as a plane deformation process. Therefore, considering

the plane deformation state at the entrance, the following is derived from the generalized Hooke's law:

$$\begin{aligned} \sigma_x &= \sigma_b \\ \sigma_y &= \nu_s (\sigma_x + \sigma_z) \\ \varepsilon_z &= \frac{1}{E_s} [\sigma_z - \nu_s (\sigma_x + \sigma_y)] \end{aligned} \tag{3}$$

From Eq. (3), the strain in the thickness direction at the entrance is

$$\varepsilon_z = \frac{1 - \nu_s^2}{E_s} (\sigma_z - \frac{\nu_s}{1 - \nu_s} \sigma_b) \tag{4}$$

Similarly, the strain in the thickness direction at the exit side is obtained. The thicknesses Δh_{in} and Δh_{out} of elastic zone I and zone III are derived as follows:

$$\Delta h_{in} = \frac{1 - \nu_s^2}{E_s} h_{in} (\sigma_{sin} - \frac{\nu_s}{1 - \nu_s} \sigma_b) \tag{5}$$

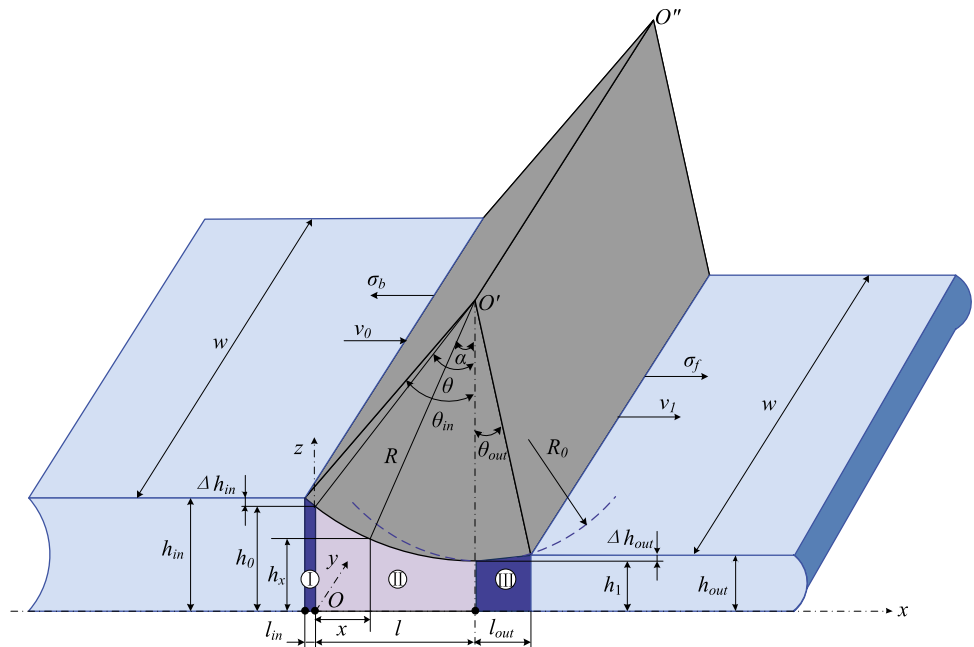
$$\Delta h_{out} = \frac{1 - \nu_s^2}{E_s} h_{out} (\sigma_{sout} - \frac{\nu_s}{1 - \nu_s} \sigma_f) \tag{6}$$

where σ_{sin} and σ_{sout} are the strip deformation resistance at the entrance and exit sides, respectively; σ_f and σ_b are the forward and backward tension stresses, respectively, and E_s and ν_s are the Young's modulus and Poisson ratio of the strip, respectively.

Therefore, the projected lengths of the roll-strip contact arcs l_{in} and l_{out} in elastic zone I and zone III, respectively, are:

$$l_{in} = \sqrt{2R(\Delta h + \Delta h_{in})} - \sqrt{2R\Delta h} \tag{7}$$

Fig. 2 Division of the deformation zone in the roll gap



$$l_{out} = \sqrt{2R\Delta h_{out}} \tag{8}$$

The flattened roll radius is:

$$R=R_0 \left[1 + \frac{4(1-\nu_w^2)}{\pi E_w w} \frac{F}{(\sqrt{\Delta h} + \Delta h_t + \Delta h_{out} + \sqrt{\Delta h_{out}})^2} \right] \tag{9}$$

where E_w and ν_w are the Young’s modulus and Poisson ratio of the work roll, respectively, and F is the total rolling force.

2.2 Friction heat in elastic zone

In a hot roughing mill, the strip is stuck to the roll in the deformation zone, resulting in a relative non-sliding zone between the strip and the roll in a large range of the roll gap. Therefore, the frictional heat generated by the relative sliding of the strip and roll in hot rolling can be neglected. In contrast to hot rolling, the lubrication state of deformation is good in the cold rolling process. Except for the neutral point and a tiny range near it, relative sliding between the strip and the roll occurs, and the friction heat needs to be calculated. In the present paper, the friction heat generated in the plastic deformation zone and the elastic zone is calculated, and the roll force of elastic deformation zone I F_{in}^e is:

$$\begin{aligned} F_{in}^e &= 2w \int_{-l_{in}}^0 \left(\frac{E_s}{1-\nu^2} \frac{h_{in}-h_x}{h_{in}} + \frac{\nu_s}{1-\nu_s} \sigma_b \right) dx \\ &= 2w \int_{\theta_{in}}^{\theta} \left(\frac{E_s}{1-\nu^2} \frac{h_{in}-h_{\alpha}}{h_{in}} + \frac{\nu_s}{1-\nu_s} \sigma_b \right) (-R \cos \alpha d\alpha) \\ &= \frac{2E_s w R}{(1-\nu^2) h_{in}} \left[(h_{in}-R-h_1)(\sin \theta_{in}-\sin \theta) + \frac{R}{2} \left(\theta_{in}-\theta + \frac{\sin 2\theta_{in}-\sin 2\theta}{2} \right) \right] \\ &\quad + \frac{2R w \nu_s \sigma_b}{1-\nu_s} (\sin \theta_{in}-\sin \theta) \end{aligned} \tag{10}$$

The roll force of elastic deformation zone III F_{out}^e is:

$$\begin{aligned} F_{out}^e &= 2w \int_l^{l+l_{out}} \left(\frac{E_s}{1-\nu^2} \frac{h_{out}-h_x}{h_{out}} + \frac{\nu_s}{1-\nu_s} \sigma_f \right) dx \\ &= 2w \int_0^{-\theta_{out}} \left(\frac{E_s}{1-\nu^2} \frac{h_{out}-h_{\alpha}}{h_{out}} + \frac{\nu_s}{1-\nu_s} \sigma_f \right) (-R \cos \alpha d\alpha) \\ &= \frac{2E_s w R}{(1-\nu^2) h_{out}} \left[(h_{out}-R-h_1) \sin \theta_{out} + \frac{R}{2} \left(\theta_{out} + \frac{\sin 2\theta_{out}}{2} \right) \right] + \frac{2R w \nu_s \sigma_f}{1-\nu_s} \sin \theta_{out} \end{aligned} \tag{11}$$

where $\theta = \sin^{-1}(l/R)$, $\theta_{in} = \sin^{-1}[(l_{in}+l)/R]$, and $\theta_{out} = \sin^{-1}(l_{out}/R)$.

Note that the frictional power generated by the friction between the roll and strip is:

$$\dot{W}_f^e = \mu F^e \bar{v}_r \tag{12}$$

where \bar{v}_r is the average value of the absolute relative velocity of the roll and strip, F^e is the rolling force in the elastic zone, and μ is the friction coefficient. If the relative speed at the bite point of the strip is approximately linear, \bar{v}_r can be expressed as:

$$\bar{v}_r = \frac{v_R}{2} \cdot \frac{f^2 + b^2}{f + b} \tag{13}$$

$$b = 1 - (1+f)(1-r) \tag{14}$$

where f is the forward slip rate, b is the backward slip rate, and r is the reduction ratio.

The heat generated by friction work in the elastic zone is:

$$Q_f^e = A \dot{W}_f^e t_r^e \tag{15}$$

where A is the thermal equivalent of the work, t_r^e is the contact time between the roll and strip in the elastic zone, and $t_r^e = \sqrt{R(\Delta h_{in} + \Delta h_{out})} / v_R$.

Therefore, the frictional heat in the elastic zone of the

roll gap is determined by Eqs. (10), (11), (12) and (15),

which is distributed to the work roll and strip with a certain proportion.

2.3 Deformation heat in the plastic zone

2.3.1 Exponential velocity field

The deformation heat in the plastic zone is calculated by the energy method and the UY criterion. The deformation in the width direction was neglected because the shape factor of the strip ensures that the width-to-thickness ratio is greater than 10 in the cold rolling process [14]. A new exponential velocity field is established.

$$\begin{aligned} v_x &= v_0 e^{1-\frac{h_x}{h_0}} \\ v_y &= v_0 h'_x \left(\frac{1}{h_0} - \frac{1}{h_x} \right) e^{1-\frac{h_x}{h_0}} y \\ v_z &= v_0 \frac{h'_x}{h_x} e^{1-\frac{h_x}{h_0}} z \end{aligned} \tag{16}$$

Based on the Cauchy equation [15], the strain rate field in zone II is derived as follows:

$$\begin{aligned} \dot{\epsilon}_x &= \frac{\partial v_x}{\partial x} = -\frac{v_0 h'_x}{h_0} e^{1-\frac{h_x}{h_0}} \\ \dot{\epsilon}_y &= \frac{\partial v_y}{\partial y} = v_0 h'_x \left(\frac{1}{h_0} - \frac{1}{h_x} \right) e^{1-\frac{h_x}{h_0}} \\ \dot{\epsilon}_z &= \frac{\partial v_z}{\partial z} = v_0 \frac{h'_x}{h_x} e^{1-\frac{h_x}{h_0}} \end{aligned} \tag{17}$$

From Eqs. (16) and (17), $v_x|_{x=0} = v_0$, $v_y|_{y=0} = 0$, $v_z|_{z=h_x} = -v_x \tan \alpha$; $v_x|_{x=l} = v_0 \cdot e^{1-\frac{h_1}{h_0}}$; $v_y|_{x=l} = 0$; $v_z|_{x=l} = 0$; $\dot{\epsilon}_x + \dot{\epsilon}_y + \dot{\epsilon}_z = 0$. These equations satisfy the boundary. Thus, Eqs. (16) and (17) are the kinematically admissible velocity and strain-rate field, respectively.

2.3.2 Unified yield criterion

The UY criterion is a unified expression of various linear yield criteria in the error triangle between Tresca’s and the twin shear-stress (TSS) yield loci in the π - plane [16], as shown in Fig. 3. The UY criterion is usually expressed as

$$\begin{cases} \sigma_1 - \frac{d\sigma_2}{1+d} - \frac{\sigma_3}{1+d} = \sigma_s & \text{if } \sigma_2 \leq \frac{\sigma_1 + \sigma_3}{2} \\ \frac{\sigma_1}{1+d} + \frac{d\sigma_2}{1+d} - \sigma_3 = \sigma_s & \text{if } \sigma_2 \geq \frac{\sigma_1 + \sigma_3}{2} \end{cases} \tag{18}$$

where d is the yield-criterion parameter, which represents the effect of the intermediate principal shear stress on the yield of the materials, and $0 \leq d \leq 1$. σ_1, σ_2 , and σ_3 are principal stresses.

Zhao derived the specific plastic work rate per unit volume of the UY criterion [17]:

$$D(\dot{\epsilon}_{ij}) = \frac{1+d}{2+d} \sigma_s (\dot{\epsilon}_{\max} - \dot{\epsilon}_{\min}) \tag{19}$$

where $\dot{\epsilon}_{\max}$ and $\dot{\epsilon}_{\min}$ are the maximum and minimum strain rates, respectively, during deformation, $\dot{\epsilon}_{\max} = \dot{\epsilon}_x$, and $\dot{\epsilon}_{\min} = \dot{\epsilon}_z$.

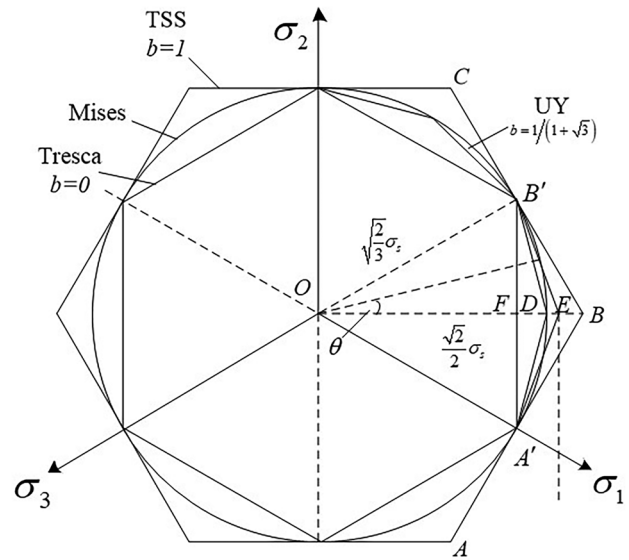


Fig. 3 Yield loci in the π - plane

The UY criterion was applied to the optimization of the force and energy parameters in plastic processing in a preliminary study by the authors [18]. This motivated the authors to use the UY criterion in this paper to optimize the calculation accuracy of the deformation heat in the cold rolling process.

2.3.3 Deformation heat

By substituting Eq. (17) into Eq. (19), the inter-deformation power can be derived as follows:

$$\begin{aligned} \dot{W}_i &= \int_V D(\dot{\epsilon}_{ij}) dV = \frac{4(1+b)\sigma_s}{2+b} \int_0^l \int_0^w \int_0^{h_x} (\dot{\epsilon}_{\max} - \dot{\epsilon}_{\min}) dx dy dz \\ &= \frac{4(1+b)\sigma_s}{2+b} \int_0^l \int_0^w \int_0^{h_x} \left\{ -\frac{v_0 h'_x}{h_0} e^{1-\frac{h_x}{h_0}} - v_0 \frac{h'_x}{h_x} e^{1-\frac{h_x}{h_0}} \right\} dx dy dz \\ &= \frac{4(1+b)\sigma_s}{2+b} U \left[\left(2 + \frac{h_1}{h_0} \right) e^{1-\frac{h_1}{h_0}} - 3 \right] \end{aligned} \tag{20}$$

The flow volume per second is $U = v_0 h_0 w = v_1 h_1 w = v_n h_n w = v_R \cos \alpha_n (R + h_1 - R \cos \alpha_n)$, and α_n is the neutral angle.

Therefore, the heat generated by strip plastic deformation is:

$$Q_i = A \eta \dot{W}_i t_r^p \tag{21}$$

where η is the coefficient of heat conversion from plastic work to heat ($\eta=0.95 \sim 0.98$ [19]), t_r^p is the contact time between the roll and strip in the plastic zone, and $t_r^p = \sqrt{R(\Delta h)} / v_R$. Incidentally, because plastic deformation heat is generated inside the strip and the contact time

between the work roll and strip is short, it is assumed that only 3% of the deformation heat is transferred to the work roll [20].

2.4 Friction heat in plastic zone

Friction only acts on the interface between the roll and strip. It is noted that the friction stress $\tau_f = \mu k = \mu \sigma_s / \sqrt{3}$ and the velocity discontinuity Δv_f are always in the same direction, as shown in Fig. 4, and the friction power is then deduced using the collinear vector inner product (see the Appendix for details):

$$\dot{W}_f^p = 4\mu k w R \left\{ v_R (\theta - 2\alpha_n) + \frac{U}{h_0 w} \left[g_b \ln \frac{(1 + \cos \alpha_n + \sin \alpha_n)(1 + \cos \theta - \sin \theta)}{(1 + \cos \alpha_n - \sin \alpha_n)(1 + \cos \theta + \sin \theta)} + g_f \ln \frac{1 + \cos \alpha_n + \sin \alpha_n}{1 + \cos \alpha_n - \sin \alpha_n} \right] \right\} \quad (22)$$

where g_b and g_f are the parameters of the backward and forward slip zones, respectively, $g_b = e^{-\frac{h_{mb}}{h_0}}$, $g_f = e^{-\frac{h_{mf}}{h_0}}$, h_{mb} and h_{mf} are the average thicknesses of the backward and forward slip zones, respectively, $h_{mb} = \frac{h_0 + h_{a0}}{2}$, and $h_{mf} = \frac{h_1 + h_{a1}}{2}$.

The friction coefficient μ reflects the friction degree between the strip and roll. The friction coefficient is mainly related to the lubrication characteristics of the emulsion, rolling speed, state of the roll surface, and roll material during the cold rolling process. By taking the above factors into consideration, the friction coefficient was calculated as follows [21]

$$\mu = \left[\mu_0 + \mu_V \cdot e^{-\frac{v_R}{V_0}} + \mu_r (r_a - r_{a0}) \right] \left(1 + \frac{s_0}{s_1 s} \right) \left(1 + \eta_1 \ln \frac{h_{in} - h_{out}}{\eta_0 h_{in}} \right) \quad (23)$$

where μ_0 is the basic value of the friction coefficient, μ_V is the speed influence factor of the friction, V_0 is the basic

speed, μ_r is the roughness influence factor of the friction, r_a is the roll roughness, r_{a0} is the basic roll roughness, s is the roll wear, s_0 and s_1 are the wear influence factors of the friction, and η_0 and η_1 are the reduction influence factors of the friction.

Therefore, the heat generated by friction work per unit area in the plastic zone is

$$Q_f^p = A \dot{W}_f^p t_r^p \quad (24)$$

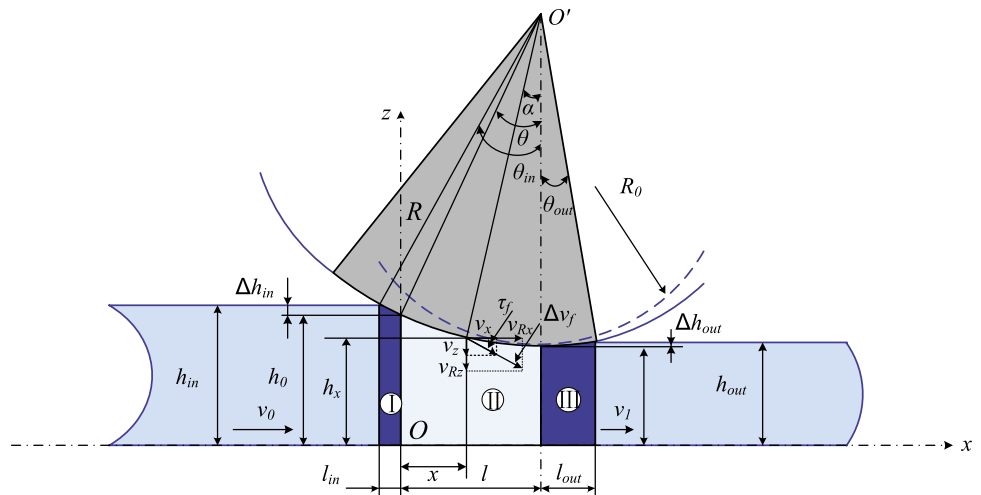
According to Bullock’s theory, when relative motion between the roll and strip occurs, some heat q will transfer to the roll surface by a constant dimensionless ratio κ , and

the rest of the heat will transfer to the strip surface by $(1 - \kappa)$ at the same time. In the cold rolling process, the materials of the roll and strip are similar, the speed is almost the same, and $\kappa \approx 0.5$. Therefore, the frictional heat generated in the roll gap during the cold rolling process can be considered to be evenly distributed between the strip and the work roll.

3 Heat exchange of work roll during cold rolling process

In the cold rolling process, when the work roll rotates, the surface of the roll is first in contact with the strip. Under the joint action of plastic deformation work and friction heat, the temperature of the roll surface rises rapidly. In addition, in the convection between the work roll, air and emulsion, the heat conduction occurring between the work roll and the

Fig. 4 τ_f and Δv_f on the interface between the roll and strip



intermediate roll will reduce the temperature of the roll surface, and then periodically change until the temperature of the work roll reaches a dynamic balance. Therefore, to accurately predict the temperature of the work roll, the heat loss of the roll should be considered comprehensively in addition to accurately calculating the heat source of the roll gap.

3.1 Convection heat transfer between work roll and emulsion

The heat transfer mode between the work roll and the emulsion is heat convection, so it satisfies Newton's law of convective heat transfer. The heat taken away by the emulsion is expressed as follows:

$$Q_e = (T_w - T_e)l_{we}w_r h_e t_{we} \quad (25)$$

where T_w and T_e are the temperatures of the work roll and emulsion, respectively, l_{we} is the contact arc length between the work roll and emulsion, w_r is the length of the work roll, h_e is the emulsion heat transfer coefficient and t_{we} is the contact time between the roll and the emulsion.

The emulsion heat transfer coefficient h_e is directly related to the concentration, flow rate, and injection mode. Many studies have shown that the heat transfer coefficients of emulsions decrease with increasing emulsion content. Therefore, the relationship between h_e and the emulsion flow density ω , the temperature of the work roll's surface T_s , and the emulsion concentration C was determined through multiple regression to be the following

$$h_e = k_0 \omega^a T_s^b \exp(c + dC) \times 1.163 \quad (26)$$

Then, according to Eq. (26), based on the laboratory experiment and online measured data, the values of the parameters in Eq. (26) were as follows: $k_0 = 0.3$, $a = 0.264$, $b = -0.213$, $c = 9.45$, and $d = -19.18$.

3.2 Convection heat transfer between work roll and air

The heat exchange between the work roll and air was calculated from the following equation:

$$Q_a = (T_w - T_a)l_{wa}w_r h_a t_{wa} \quad (27)$$

where T_a is the temperature of the air, l_{wa} is the contact arc length between the work roll and the air, h_a is the air heat transfer coefficient, and t_{wa} is the time of heat exchange.

3.3 Heat exchange between work roll and intermediate roll

Because of the temperature difference of each roll in the cold rolling process, the heat passes from the work roll to

the intermediate roll, which is a heat loss problem of the work roll. Since the roll contact heat transfer mode is heat conduction, it can be calculated according to Fourier's law of heat conduction as follows:

$$Q_{inter} = \frac{2(T_w - T_i)l_{wi}b_w b_i w_r t_{wi}}{\sqrt{t_{wi}}\pi(b_w + b_i)} \quad (28)$$

where T_i is the temperature of the intermediate roll, b_w and b_i are the heat storage coefficients of the work roll and the intermediate roll respectively, t_{wi} is the contact time between the work roll and intermediate roll, and l_{wi} is the contact arc length between the work roll and the intermediate roll. l_{wi} is calculated as follows

$$l_{wi} = 2.256 \sqrt{p_{wi}} \sqrt{8.0 \frac{1 - \nu^2}{\pi} \frac{(E_w + E_i)(D_w D_i)}{(E_w E_i)(D_w + D_i)}} \quad (29)$$

where p_{wi} is the contact pressure between the work roll and the intermediate roll, and the data can be obtained by real-time feedback in the cold rolling field, E_i is the Young's modulus of the intermediate roll, and D_w and D_i are the diameters of the work roll and the intermediate roll, respectively.

3.4 Temperature rise of work roll during cold rolling

According to the law of conservation of energy, the heat source causing the temperature rise of the work roll is shown as follows:

$$Q_s = \kappa(Q_f^e + Q_f^p) + 0.03Q_i - Q_e - Q_a - Q_{inter} \quad (30)$$

where Q_s is the energy causing the temperature rise of the work roll. The relationship between Q_s and the temperature change rate is

$$\frac{\partial T}{\partial t} = Q_s / \rho_w c_w \Delta V_w \Delta t \quad (31)$$

where ρ_w is the work roll's density, c_w is the work roll's specific heat, ΔV_w is the volume of the work roll unit and Δt is the time of temperature change. Considering that the surface temperature change rate of the roll was the largest, this change rate decreases gradually as it approaches the center of the roll. This is because the outer layer of the work roll is in direct contact with the strip, resulting in a relatively rapid temperature change on the surface of the work roll. Therefore, the work roll is divided into cells along the radial direction, and the thickness of the outermost cell is the smallest, as shown in Fig. 5.

Because of the small volume of the work roll unit and the short temperature change time, Eq. (31) is rewritten as follows:

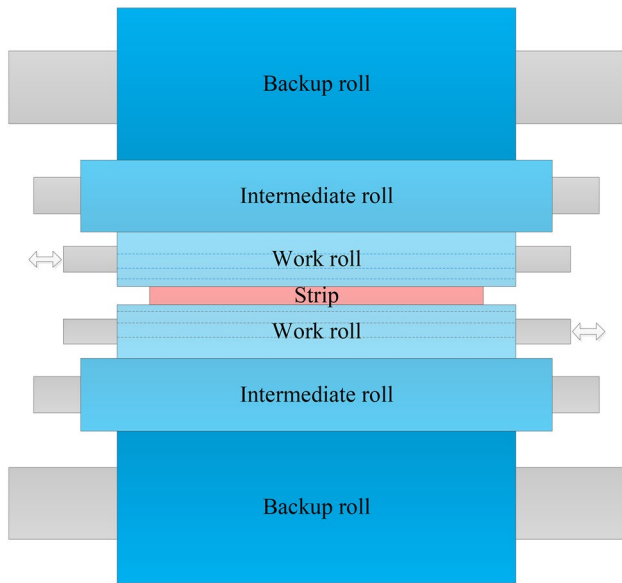


Fig. 5 Element division along the radial direction of the work roll

$$\Delta T = Q_s / (\rho_w c_w \Delta V_w) \tag{32}$$

By substituting Eq. (30) into (32), the temperature rise of the work roll in the cold rolling process is obtained. In the specific calculation of the roll temperature, Eq. (32) was used to first obtain the temperature change in a given time, and the temperature was incremented by 3 °C until the temperature of the work roll was stable.

4 Results and industrial verifications

To validate the temperature prediction model of the cold rolling work roll proposed in this paper, the authors collected a large amount of actual measurement data in the cold rolling production line of a Chinese steel company. This cold tandem rolling mill group comprised five UCM rolling

Table 1 Comparison of work roll temperature calculated by the present model with the measured one

Instance no.	1	2	3	4	5
$2h_{in}/mm$	1.720	1.248	1.177	0.828	0.634
$2h_{out}/mm$	1.150	1.210	0.991	0.683	0.5
$\epsilon/\%$	33.14%	3%	16.9%	17.5%	21.1%
σ_s/MPa	652.09	738.32	746.65	776.8	823.7
R_0/mm	212.41	217.15	212.2	212.2	194.52
R/mm	329.92	436.80	443.94	463.7	490.6
$v_R/m/s^{-1}$	15.53	13.5	15.48	18.4	20.25
$\omega/L \cdot \min^{-1} \cdot m^{-1}$	7.33	5.86	6.47	6.59	7.00
$h_c/J/(s \cdot m^2 \cdot K)$	4109	3873	3975	3995	4059
p_w/kN	1034	803	987	1007	1025
σ_f/kN	87.22	45.08	58.8	45.08	30.38
σ_b/kN	123.48	157.78	175.42	137.2	107.8
μ	0.037	0.042	0.034	0.048	0.039
Calculated temperature/°C	66.5	54.46	62.3	61.1	65.3
Measured temperature/°C	64.8	53.03	60.64	59.27	63.9
Error/%	2.62%	2.7%	2.74%	3.1%	2.19%

stands and was equipped with various detection instruments. Figure 6 shows the mill layout and instrument arrangement.

With the material of the SPCC (steel plate cold common) steel product as an example, numerous typical rolling process parameters were measured in the cold rolling field, and five groups of these data were selected to verify the calculation accuracy of the proposed model, as shown in Table 1. The density of the work roll was 7850 kg/m³, the specific heat was 490 J/(kg·K), and the initial temperature was 30 °C. Meanwhile, the emulsion’s temperature was 55 °C, the concentration of the emulsion was 5%, the cover angle of the emulsion nozzle was 65°, and the contact angle between the work roll and intermediate roll was 6°. The heat transfer coefficient of air cooling is between 114 and 230 J/(s·m²·K), and 200 J/(s·m²·K) was selected in this work [10].

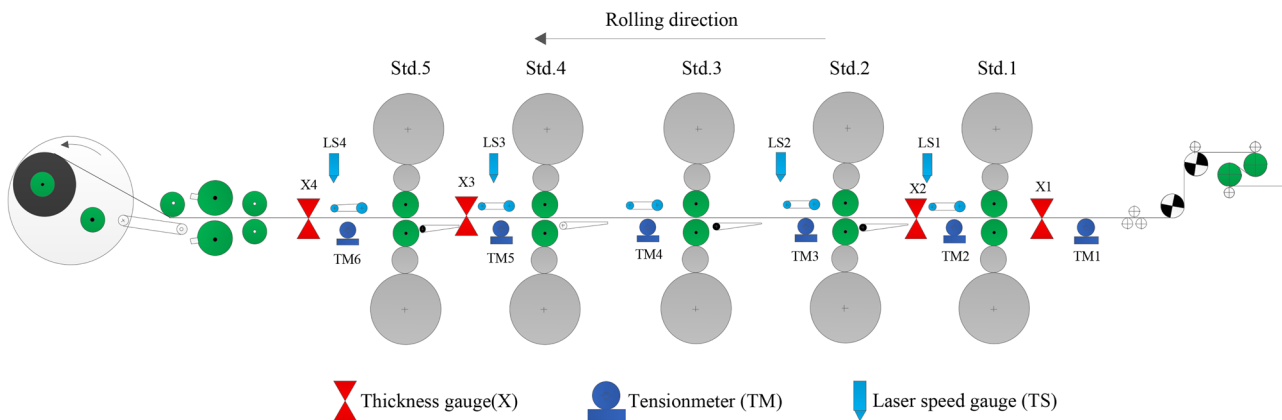


Fig. 6 Layout of 1450-mm cold tandem mill and instrument arrangement

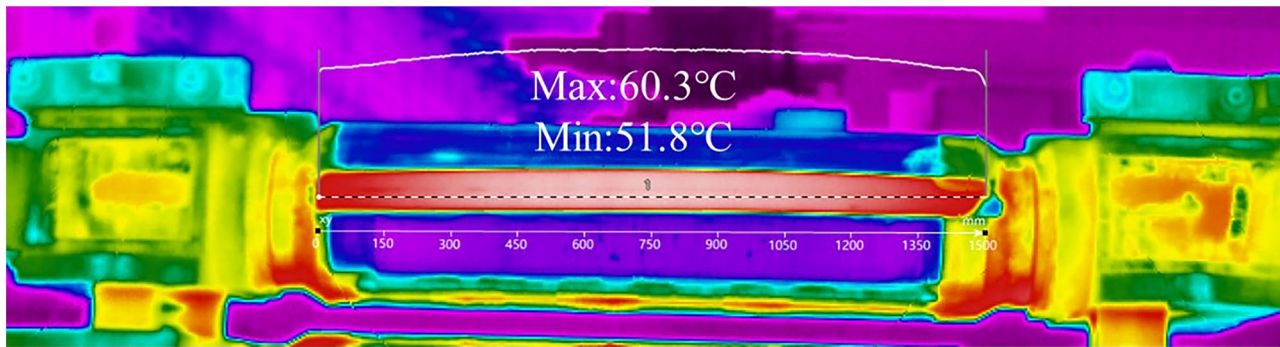


Fig. 7 Lateral temperature distribution of the work roll measured by the thermal imager

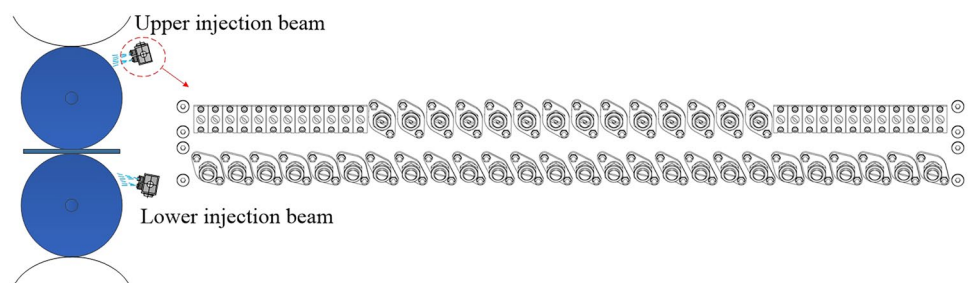
The calculated values were compared with the actual temperature values monitored by the thermal imager, by repeatedly optimizing the value of d (yield-criterion parameter). The error between the calculated temperature and actual measured data was within 3.1% when $d=0.816$, as shown in Table 1. In addition, the authors also used TSS and ID (inscribed dodecagon of the von Mises yield locus) yield criterion for calculating the work roll temperature, with maximum errors of 5.4% and 6.8%, respectively, as shown in Fig. 9. This indicated that the application of the UY criterion could effectively improve the calculation accuracy of the work roll temperature. Incidentally, the measured work roll temperature in Table 1 was the average value within the width of the strip, and Fig. 7 shows the data output by the thermal imager. To avoid the error of the measurement result caused by roll reflection, thermally sensitive tape was attached to the surface of the roll, which is shown by the red strip in Fig. 7. It is worth mentioning that since the off-line temperature of the work roll was measured immediately after the roll change, the cooling effect of the residual emulsion on the work roll still existed, but there was no deformation heat or friction heat; so, the measured temperature was lower than the calculated value.

Note that the measured axial temperature of the work roll in Fig. 7 showed a flat bell-shaped distribution, which was caused by the selective coolant system changing the emulsion flow distribution along the axial direction of the roll. Figure 8 shows the layout of the coolant nozzles for

stand 5 of a 1450 mm tandem cold rolling mill, with two upper and lower jet beams. Each jet beam contained two rows of nozzles, and 26 constant flow valves in the lower row for basic work roll cooling and lubrication, as well as 14 servo valves and 24 mini-servo valves in the upper row for selective cooling to control the thermal crown of the work roll. The cooling range of each servo valve was 52 mm, and the cooling range of the mini-servo valve was 26 mm, which corresponded to the flatness measurement section width.

Therefore, to further verify the accuracy of the temperature prediction model in this paper, the heat transfer coefficient for each nozzle cooling range was calculated according to the emulsion flow of all the nozzles in a certain pass. The temperature distribution in the width direction of the work roll was calculated by substituting the process parameters into the temperature prediction model, and the comparison with the measured data is shown in Fig. 9. The authors also used the FEM to simulate the temperature field of the work roll with the same process parameters, and the calculation results are also shown in Fig. 9. Since the coolant plan used in this pass had a secondary parabolic distribution, the temperature distribution in the width direction of the work roll was also a secondary parabolic shape. Each calculated temperature value in Fig. 9 corresponds to the control area of the emulsion nozzle, and the temperature distribution trend was in good agreement with the measured data. The comparison between the theoretical model calculation results and the FEM simulation results showed

Fig. 8 Coolant nozzle layout of stand. 5 of a 1450-mm tandem rolling mill



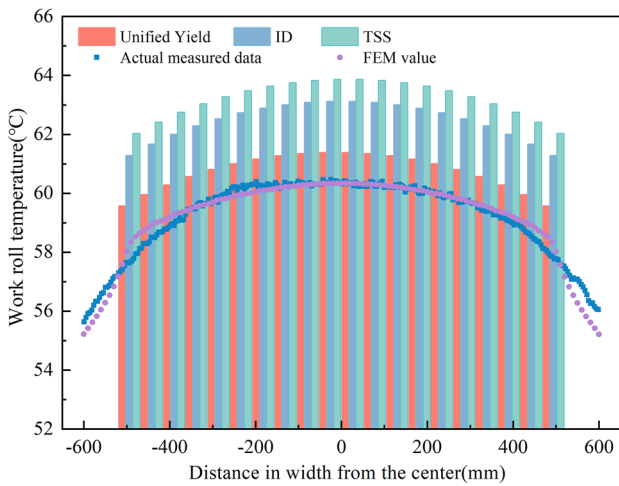


Fig. 9 Comparison of the predicted and measured work roll temperature distributions

that when the boundary conditions were set reasonably, the FEM had a higher calculation accuracy, but the calculation time of each FEM model was 12 h, while the calculation of the theoretical model was only a few minutes. The calculated temperatures were larger than the measured temperatures and FEM simulation results because the temperature prediction model in this paper was based on the upper bound principle.

5 Discussion

Based on the deformation heat model, given by Eq. (20) and the friction heat model given by Eqs. (14) and (23), the influences of different rolling process parameters on the deformation heat and friction heat were studied, and the results are shown in Fig. 10a–c.

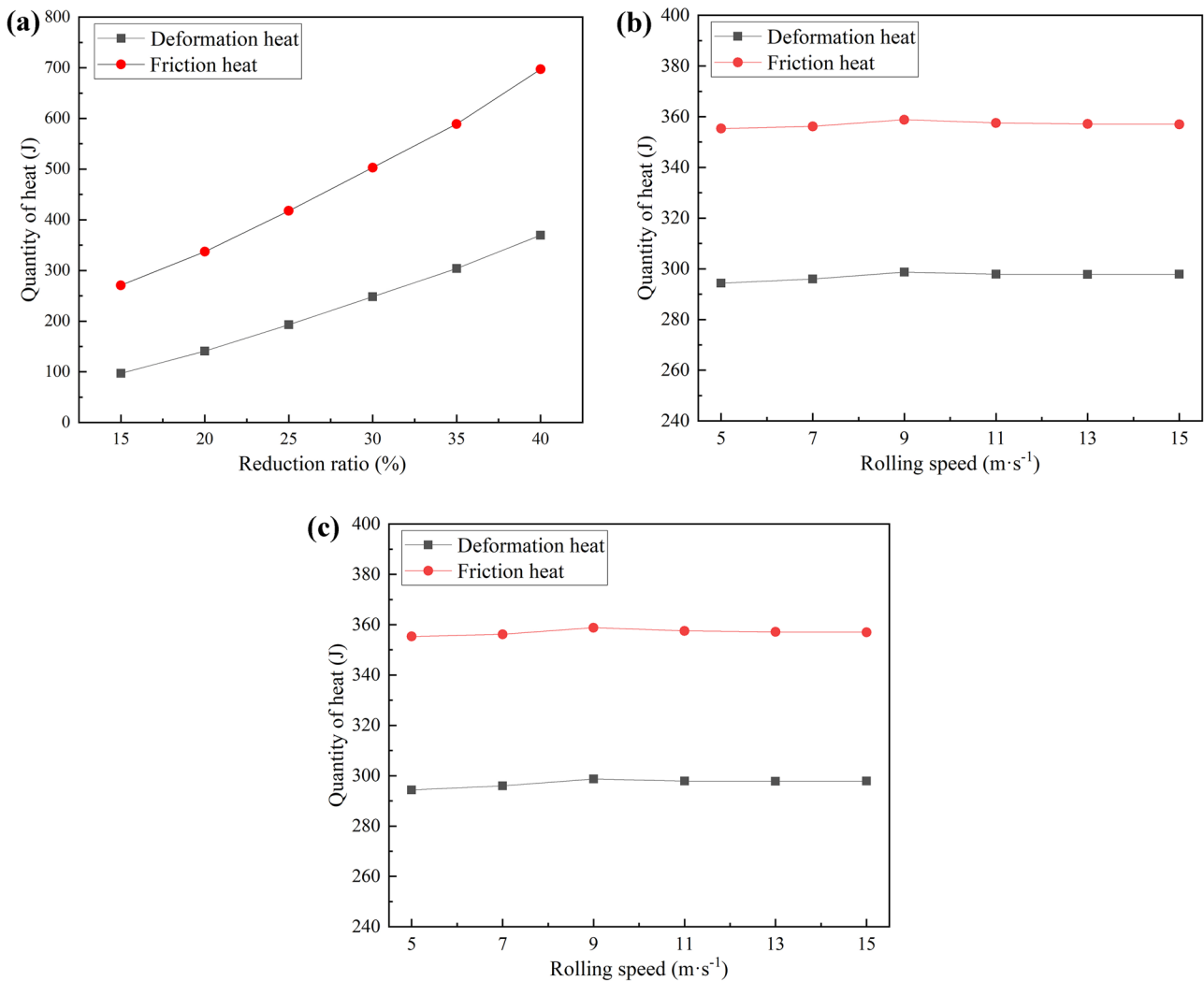


Fig. 10 Influences of different rolling process parameters on the deformation heat and friction heat. **a** reduction ratio, **b** rolling speed, and **c** deformation resistance

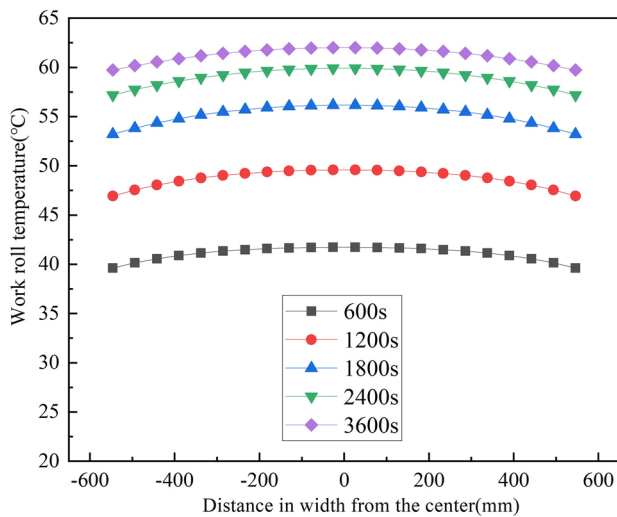


Fig. 11 Variation of the work roll temperature field with time

Figure 10a shows the significant increase in the deformation heat and friction heat during the cold rolling process with increasing reduction ratio. This was caused by the increasing volume of the deformed metal, resulting in the rolling force and friction becoming larger and causing an increase in the deformation heat and friction heat. Therefore, the stability of the thermal crown of the work roll of each stand can be ensured by reasonably distributing the reduction ratio of each stand. In Fig. 10b, the deformation heat and friction heat were basically unchanged with increasing rolling speed, and their values fluctuated only slightly. This was because, when only v_0 increased, the inter-deformation power and friction power increased significantly, but the contact time between the work roll and the strip in the roll gap also decreased significantly, which resulted in a constant deformation heat and friction heat. The deformation resistance of the strip is another key parameter that was studied in the present work. According to the calculation results shown in Fig. 10c, the deformation heat and friction heat increased significantly with the increase in the strip deformation resistance. In addition, the change in the cold rolling friction heat caused by the change in the strip deformation resistance was more significant than the change in the deformation heat.

To understand the change of the work roll temperature field of the cold rolling more clearly, the temperature prediction model in this paper was used to calculate the distributions of the work roll temperature along the width direction at different time periods at the beginning of rolling, and the results are shown in Fig. 11. The results showed that the temperature of the work roll increased rapidly in the initial stage of rolling, and the

temperature rise of the work roll center reached $11.73\text{ }^{\circ}\text{C}$ in the stage from 0 to 600 s from the start of rolling. As the cold rolling progressed, the temperature rise of the work roll began to gradually decrease. In the stage from 2400 to 3600 s at the beginning of cold rolling, the temperature rise of the work rolls was only $2.1\text{ }^{\circ}\text{C}$, and the temperature of the work roll reached dynamic equilibrium after 3600 s of the start of rolling. This result was directly related to the properties of the emulsion and the actual rolling process parameters for this pass. It is worth emphasizing that, in the changing stage of the temperature field of the work roll, the thermal crown will change and then the shape of the loaded roll gap will be changed, which will lead to fluctuations in the shape of the cold rolling strip. Therefore, by controlling the distribution and temperature of the emulsion to preheat the work roll locally, the temperature field of the roll and the hot roll shape will be closer to the stable state, which can effectively shorten the time for the work roll temperature field to reach dynamic equilibrium, and then improve the shape quality of cold rolling strip. The temperature prediction model established in this paper can be effectively used as a basis for regulating the temperature field of a cold rolling work roll.

6 Conclusions

1. Based on the new exponential velocity field, an energy method was proposed by establishing an analytical solution of the internal deformation heat in the plastic zone during the cold rolling process. Considering the influence of tension, the deformation zone was divided precisely, and friction heat analytical solutions in the elastic zone and plastic zone were established. By comprehensively considering the heat exchange between the work roll and the emulsion, air, and intermediate roll, a temperature calculation model of the cold rolling work roll was established. The accuracy of the model was verified by industrial measured data, and the maximum error was within 3.1% when the yield parameter $d=0.816$. The prediction of the temperature distribution is in good agreement with the measured curve and the FEM results.
2. The deformation resistance and the reduction ratio could cause significant changes in the frictional heat and deformation heat. The frictional heat was far greater than the deformation heat, which was relatively stable during cold strip rolling. With increasing rolling speed, the inter-deformation power and friction power increased, but the deformation heat

and friction heat did not change with rolling speed because the contact time between the work roll and the strip became shorter.

3. The influence of the rolling time on the temperature field of the work roll in the cold rolling was studied through the temperature prediction model. In the early stage of cold rolling, the work roll was heated rapidly because of deformation heat and friction heat. As rolling progressed, since the heat input and heat output of the work roll gradually reached a dynamic balance, the temperature field tended to be stable after cold rolling for 3600 s.

Appendix

According to the collinear vector inner product, the friction power \dot{W}_f^p is

$$\begin{aligned} \dot{W}_f &= 4 \int_0^l \int_0^w \tau_f |\Delta v_f| dF = 4 \int_0^l \int_0^w \tau_f \Delta v_f dF = 4 \int_0^l \int_0^w (\tau_{fx} \Delta v_x + \tau_{fy} \Delta v_y + \tau_{fz} \Delta v_z) dF \\ &= 4mk \int_0^l \int_0^w (\Delta v_x \cos \alpha + \Delta v_y \cos \beta + \Delta v_z \cos \gamma) dF \end{aligned} \tag{33}$$

where α , β , and γ are the angles between τ_f and the directions of the x , y , and z axes.

Since the tangential velocity discontinuity Δv_f and the tangent of the roll surface have the same direction, the values of the direction cosines were determined by Eq. (1), and they are

$$\cos \alpha = \pm \frac{\sqrt{R^2 - (l-x)^2}}{R}, \cos \gamma = \pm \frac{(l-x)}{R} = \sin \alpha, \cos \beta = 0 \tag{34}$$

The differential element of the roll surface from Eq. (2) is

$$dF = \sqrt{1 + (h'_x)^2} dx dy = \sec \alpha dx dy \tag{35}$$

The components of tangential velocity discontinuity Δv_f on roll surface from Eq. (16) are

$$\begin{aligned} \Delta v_x &= v_R \cos \alpha - v_0 e^{1-\frac{hx}{h_0}} \\ \Delta v_y &= -v_0 h'_x \left(\frac{1}{h_0} - \frac{1}{h_x} \right) e^{1-\frac{hx}{h_0}} y \\ \Delta v_z &= v_R \sin \alpha - v_0 \tan \alpha e^{1-\frac{hx}{h_0}} \end{aligned} \tag{36}$$

By substituting Eqs. (34), (35) and (36) into Eq. (33) and integrating, we obtain

$$\begin{aligned} \dot{W}_f &= 4\mu kw \left[\int_0^l \left(v_R \cos \alpha - v_0 e^{1-\frac{hx}{h_0}} \right) dx + \int_0^l \left(v_R \sin \alpha - v_0 \tan \alpha e^{1-\frac{hx}{h_0}} \right) \tan \alpha dx \right] \\ &= 4\mu kw (I_1 + I_2) \end{aligned} \tag{37}$$

$$\begin{aligned} I_1 &= \int_0^l \left(v_R \cos \alpha - v_0 e^{1-\frac{hx}{h_0}} \right) dx = \int_0^{x_n} \left(v_R \cos \alpha - v_0 e^{1-\frac{hx}{h_0}} \right) dx - \int_{x_n}^l \left(v_R \cos \alpha - v_0 e^{1-\frac{hx}{h_0}} \right) dx \\ &= v_R R \left(\frac{\theta}{2} - \alpha_n + \frac{\sin 2\theta}{4} - \frac{\sin 2\alpha_n}{2} \right) + g_f v_0 R \sin \alpha_n + g_b v_0 R (\sin \alpha_n - \sin \theta) \end{aligned} \tag{38}$$

Similarly,

$$\begin{aligned} I_2 &= \int_0^l \left(v_R \sin \alpha - v_0 \tan \alpha e^{1-\frac{hx}{h_0}} \right) \tan \alpha dx \\ &= \int_0^{x_n} \left(v_R \sin \alpha \tan \alpha - v_0 \tan^2 \alpha e^{1-\frac{hx}{h_0}} \right) dx - \int_{x_n}^l \left(v_R \sin \alpha \tan \alpha - v_0 \tan^2 \alpha e^{1-\frac{hx}{h_0}} \right) dx \\ &= v_R R \left(\frac{\theta}{2} - \alpha_n + \frac{\sin 2\alpha_n}{2} - \frac{\sin 2\theta}{4} \right) + g_f v_0 R \left[\ln \frac{1 + \cos \alpha_n + \sin \alpha_n}{1 + \cos \alpha_n - \sin \alpha_n} - \sin \alpha_n \right] \\ &\quad + g_b v_0 R \left[\ln \frac{(1 + \cos \alpha_n + \sin \alpha_n)(1 + \cos \theta - \sin \theta)}{(1 + \cos \alpha_n - \sin \alpha_n)(1 + \cos \theta + \sin \theta)} + \sin \theta - \sin \alpha_n \right] \end{aligned} \tag{39}$$

By substituting Eqs. (38) and (39) into Eq. (37) and integrating, Eq. (22) is given.

Author contribution Yufeng Zhang wrote the first draft of the paper. All authors revised and approved the final version of the manuscript.

Funding This study was funded by the National Natural Science Foundation of China (No. U20A20187), the LiaoNing Revitalization Talents Program (No. XLYC2007087), and the Fundamental Research Funds for the Central Universities (No. N2124007-1).

Availability of data and materials The datasets used or analyzed during the current study are available from the corresponding author on reasonable request.

Declarations

Competing interests We declare that we have no financial and personal relationships with other people or organizations that can inappropriately influence our work, there is no professional or other personal interest of any nature or kind in any product, service and/or company that could be construed as influencing the position presented in, or the review of, the manuscript entitled, “A novel analytical heat source model for cold rolling based on the energy method and unified yield criterion”.

References

- Zhang SH, Deng L, Che LZ (2022) An integrated model of rolling force for extra-thick plate by combining theoretical model and neural network model. *J Manuf Process* 75:100–109
- Lenard JG, Pietrzyk M (1989) The predictive capabilities of a thermal model of flat rolling. *Steel Res Int* 60(9):403–406
- Wang GD (1986) Flatness control and flatness theory. Metall Ind Press, Beijing
- Wilmote S, Milgnon J (1973) Thermal variations of the caber of the working rolls during hot rolling. *Metall Rep CRM* 34:17–34
- Lahoti GD, Shah SN, Altan T (1978) Computer-aided analysis of the deformations and temperatures in strip rolling. *J Eng Ind* 100(2):159–166
- Nakagawa K (1980) Heat crown of work rolls during aluminum hot rolling. *Sum Light Metals Technol Rep* 21:45–51
- Tseng AA (1984) A numerical heat transfer analysis of strip rolling. *J Heat Tran* 106(3):512–517
- Tseng AA, Tong SX, Maslen SH, Mills JJ (1990) Thermal behavior of aluminum rolling. *J Heat Tran* 112(2):301–308
- Chang DF (1990) An efficient way of calculating temperatures in the strip rolling process. *J Manu Sci E-T ASME* 120:93–100
- Zhang XL, Zhang J, Li XY, Li HX, Wei GC (2004) Analysis of the thermal profile of work rolls in the hot strip rolling process. *J Univ Sci Technol Beijing* 11(2):173–177
- Yang LP, Jiang ZY, Zhu JX, Yu HX (2018) Analysis of transient heat source and coupling temperature field during cold strip rolling. *Int J Adv Manuf Tech* 95:835–846
- Guo ZF, Li CS, Xu JZ, Liu XH, Wang GD (2006) Analysis of temperature field and thermal crown of roll during hot rolling by simplified FEM. *J Iron Steel Res Int* 13(6):27–30
- Benasciutti D, Brusa E, Bazzaro G (2010) Finite element prediction of thermal stresses in work roll of hot rolling mills. *Proc Eng* 2(1):707–716
- Zhang SH, Deng L, Wen TH, Che LZ, Yan L (2022) Deduction of a quadratic velocity field and its application to rolling force of extra-thick plate. *Comput Math Appl* 109:58–73
- Sezek S, Aksakal B, Can Y (2008) Analysis of cold and hot plate rolling using dual stream functions. *Mater Des* 29(3):584–596
- Yu MH, He LN, Liu CY (1992) Generalized twin-shear stress yield criterion and its generalization. *Chinese Sci Bull* 37(24):2085–2089
- Zhao DW, Li J, Liu XH, Wang GD (2009) Deduction of plastic work rate per unit volume for Unified yield criterion and its application. *Trans Nonferrous Met Soc China* 19:657–660
- Zhang YF, Zhao MY, Li X, Di HS, Zhou XJ, Peng W, Zhao DW, Zhang DH (2021) Optimization solution of vertical rolling force using unified-yield criterion. *Int J Adv Manuf Tech* 119:1035–1045
- Wang GD, Wang GL (1990) Iron and Steel Institute of Japan-Rolling theory and experience of the strip steel. Railway Press of China, Beijing
- Hosford WF (1983) Metal forming mechanics and metallurgy. Prentice-Hall Inc, Englewood Cliffs
- Sun J, Liu YM, Hu YK, Wang QL, Zhang DH, Zhao DW (2016) Application of hyperbolic sine velocity field for the analysis of tandem cold rolling. *Int J Mech Sci* 108–109:166–173

Publisher's note Springer Nature remains neutral with regard to jurisdictional claims in published maps and institutional affiliations.

Springer Nature or its licensor holds exclusive rights to this article under a publishing agreement with the author(s) or other rightsholder(s); author self-archiving of the accepted manuscript version of this article is solely governed by the terms of such publishing agreement and applicable law.